International Symposium
On Turbulence and Shear Flow
Phenomena (TSFP-9)
June 30 - July 3, 2015 *Melbourne, Australia*

INVESTIGATION OF THE WALL PRESSURE WAVENUMBER-FREQUENCY SPECTRUM BENEATH A TURBULENT BOUNDARY LAYER WITH PRESSURE GRADIENT

Edouard Salze, Christophe Bailly, Olivier Marsden & Daniel Juvé
Laboratoire de Mécanique des Fluides et d'Acoustique
École Centrale de Lyon
36 avenue Guy de Collongue, 69134 Écully cedex, France
christophe.bailly@ec-lyon.fr

ABSTRACT

Wall pressure fluctuations beneath a turbulent boundary layer in the presence of a mean pressure gradient are investigated in this study. The mean pressure gradient is achieved by changing the ceiling angle of a rectangular channel designed for flow-acoustic measurements. Wall pressure spectra are measured for zero-, adverse- and favorable-pressure-gradient boundary layers by using a pinhole microphone in conjunction with a high-frequency-calibration procedure. A direct measurement of the wall pressure wavenumber-frequency spectrum $\Phi_{pp}(k_1,k_2,\omega)$ is also performed with the use of a rotating linear antenna of remote microphones. The microphone array has been optimized to improve its response with respect to previous works (Arguillat *et al.*, 2010). Both aerodynamic and acoustic components of the wavenumber-frequency spectrum can thus be identified and are investigated.

INTRODUCTION

The understanding of vibrations and noise induced by wall pressure fluctuations is of great importance in hydroacoustics (Sevik, 1986; Blake, 1986), but also in aeronautical (Wilby, 1996; Graham, 1997) and more recently in automotive applications (Leclercq & Bohineust, 2002; Bremner, 2014). The motivations behind the present experimental investigation are twofold. First, a direct measurement of the wall pressure wavevector-frequency spectrum induced by a turbulent boundary layer, including both aerodynamic and acoustic components of loading, is undertaken to characterize boundary layer excitation. The aerodynamic part is associated with the indirect contribution to cabin noise through panel vibration while the acoustic part represents a direct contribution to this noise. They have thus a distinct influence on the sound transmitted. The necessary small separation distance between sensors, and the large difference in energy between the two components, make this experimental identification quite tricky (Abraham & Keith, 1998; Ehrenfried & Koop, 2008; Arguillat *et al.*, 2010; Gabriel *et al.*, 2014). Mainly the incompressible part of spectra has been reported over the past fifty years (Keith *et al.*, 1992; Bull, 1996). It must be mentioned that similar difficulties are also encountered in numerical simulations (Hu *et al.*, 2006; Gloerfelt & Berland, 2013; Kremer *et al.*, 2014) for extracting the acoustic component. Second, zero-pressure-gradient turbulent boundary layers are often considered. Only a fragmented view is currently offered regarding pressure gradient effects, even for modelling the aerodynamic loading (Schloemer, 1967; McGrath & Simpson, 1987; Cipolla & Keith, 2000).

The ultimate goal of the present work is to characterize 2-D wavevector-frequency spectra in various flow conditions, and to separate in each case the aerodynamic and the acoustic contributions, as they known to have a distinct influence on the transmitted sound in vibroacoustics. In a previous study by Arguillat *et al.* (2010), a rotating microphone array was used to deduce the wall pressure wavenumber-frequency spectrum through an original post-processing. Results have been reported for a turbulent boundary layer at a Reynolds number $\mathrm{Re}_{\delta_1} = u_\tau \delta_1 / \nu = 5.5 \times 10^4$ and at a moderate velocity $U_\infty = 44$ m.s^{-1}. The feasibility to estimate wavevector spectra by this original approach was demonstrated. In these expressions, u_τ denotes the friction velocity, δ_1 the displacement thickness and U_∞ the free stream velocity of the boundary layer, and ν is the kinematic viscosity of the fluid.

In the present work, wall pressure fluctuations beneath a turbulent boundary layer submitted to an external mean pressure gradient are investigated with a significantly improved experimental approach. A new channel has been developed for flow-acoustic measurements, in which the ceiling of the test section can be inclined, to generate an accelerated or decelerated mean flow over a flat plate. A new rotating microphone array, mounted on a rigid flat disk, has also been designed to enhance the spectral resolution of the wavevector-frequency spectra of wall pressure fluctuations.

EXPERIMENTAL SETUP

The experiments were conducted in the main subsonic wind tunnel of the Centre Acoustique at Ecole Centrale de Lyon in France (Panton & Robert, 1994; Arguillat *et al.*, 2010). The flow is generated by a 350 kW Neu centrifugal blower delivering a nominal mass flow rate of 15 kg.s^{-1}, and the fan is powered by an electronically controlled Tridge-Electric LAK 4280A motor. Air passes through a settling chamber including a honeycomb and several wire meshes designed to reduce free stream turbulence. Acoustic treatment on the wind tunnel walls and baffled silencers allow to reduce the noise level and to prevent contamination of acoustic measurements performed in the anechoic chamber. This results in an air flow at ambient temperature with a low

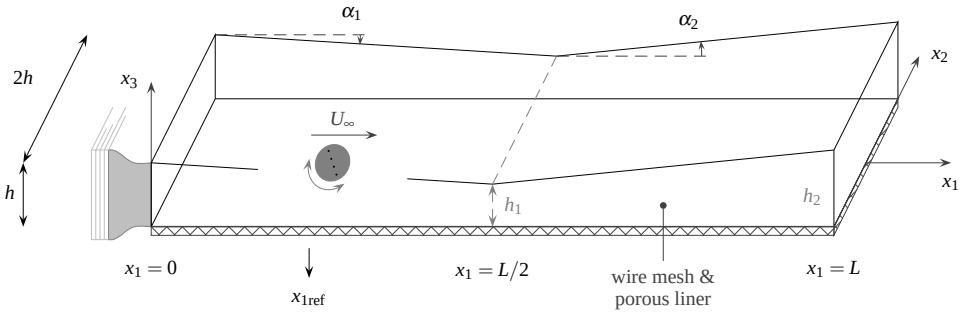

Figure 1. Sketch of the test channel and notations. The height of the initial section is $h = 250$ mm, the length of the whole channel is $L = 16h$ and the location of the disk antenna is $x_{\text{ref}} = 3h$. U_∞ is the local free stream velocity of the boundary layer at the streamwise location of the measurement, that is $x_{1\text{ref}}$ for the rotating array.

background noise and low residual turbulence intensity, less than 1%

Three configurations have been retained in the present study, corresponding to a turbulent boundary layer submitted to a zero-pressure-gradient (zpg), a favorable or negative pressure gradient (fpg) and an adverse or positive pressure gradient (apg). Each considered experimental point is denoted by the channel configuration, namely zpg or apg or fpg, which is associated with a position of the channel ceiling, see Fig. 1, and by a number associated with the free stream velocity U_∞ at the location of the disk antenna. Experimental parameters are provided in Table 1.

A detailed description of the channel can be found in Salze *et al.* (2014), including a characterization of the longitudinal mean pressure distribution, mean velocity profiles and turbulent velocity spectra, measured in various configurations.

	U_∞	$\delta_1 \times 10^3$	H	u_τ	Re_{δ_1}	Re^+	β
zpg	11	3.1	1.34	0.48	2.2×10^3	633	–
	25	2.8	1.30	1.02	4.7×10^3	1006	–
	36	3.2	1.30	1.35	7.4×10^3	1778	–
	45	3.7	1.31	1.65	1.1×10^4	2718	–
	59	3.6	1.31	2.05	1.4×10^4	3374	–
	76	2.9	1.28	2.71	1.5×10^4	3559	–
	100	3.5	1.30	3.54	2.3×10^4	5050	–
apg	8	8.4	1.38	0.31	4.6×10^3	1036	0.95
	12	8.2	1.42	0.42	6.7×10^3	1122	1.06
	19	6.2	1.41	0.66	7.9×10^3	1321	0.83
	27	5.0	1.36	0.96	9.1×10^3	1596	0.64
	38	5.5	1.31	1.34	1.4×10^4	3555	0.71
	45	5.8	1.31	1.55	1.8×10^4	5135	0.81
	57	5.2	1.31	1.95	2.0×10^4	5139	0.72
	76	6.0	1.31	2.45	3.0×10^4	8027	0.94
fpg	10	2.1	1.27	0.50	1.5×10^3	501	−0.48
	32	2.1	1.24	1.35	4.6×10^3	1353	−0.63
	45	1.7	1.23	1.90	5.0×10^3	1881	−0.50
	63	1.8	1.22	2.53	7.5×10^3	2490	−0.59

Table 1. Boundary layer parameters for the present experiments at ECL, U_∞ is the local free stream velocity, δ_1 the boundary layer displacement thickness, H the shape factor, u_τ the friction velocity, $\text{Re}_{\delta_1} = \delta_1 U_\infty/\nu$ the Reynolds number, $\text{Re}^+ = u_\tau \delta/\nu$ the Kármán number where ν is the kinematic viscosity, and $\beta = (\delta_1/\tau_w) dP_\infty/dx_1$ the Clauser parameter.

WALL PRESSURE SPECTRA

Frequency spectra have been obtained using a 1/8 microphone, fitted with a pinhole cap. The diameter of the cap hole is about $d_p \simeq 5$ mm, and the pressure spectra have been corrected to account for the spatial filtering of the sensor using the Corcos correction (Corcos, 1963). An original high-frequency calibration procedure have been performed to identify the tranfer function of the probe up to 40 kHz.

The resulting pressure spectra $S_{pp}(\omega)$ are shown in Fig. 2 as black curves for a zero pressure gradient boundary layer. The measured spectra have been normalized by mixed variables (at the top). This leads to a collapse of the spectra in the low frequency domain. They reach a maximum of about 5 dB for $\omega\delta_1/U_\infty$ around 0.4. Then, an $\omega^{-0.4}$ decay is observed in the range $0.5 < \omega\delta_1/U_\infty < 5$. Reynolds numbers are not high enough to observe the $\omega^{-0.7}$ power law. The measured spectra can also been normalized by inner variables (at the bottom). This leads to a collapse of all the spectra in the high-frequency domain $\omega\nu/{u_\tau}^2 > 0.6$, where an amplitude decay according to ω^{-5} can be distinguished. The ability of the now classical semi-empirical model of Goody (2004) to predict the shape of the pressure spectrum in a wide range of Reynolds numbers is remarkable, by fitting the experimental spectra within about 3 dB.

With reference to the zpg case, it is observed that in apg conditions, the low frequency level is increased up to 4 dB, with the position of the maximum being unchanged. In the fpg case, the low frequency level is on the contrary slightly reduced and the shape is very flat with no clear maximum observable.

The root-mean square pressure fluctuation, calculated as

$$p^2_{w,rms} = \int_0^\infty S_{pp}(\omega) d\omega$$

and normalized by viscous scaling is plotted in Fig. 3 as a function of the Reynolds number $p_w^+ = f(\text{Re}^+)$, and compared to previously published data. The normalized pressure fluctuations increase with the Reynolds number, as is the case for the previously published data. The evolution of p_w^+ with Re^+ has also been described by Farabee &

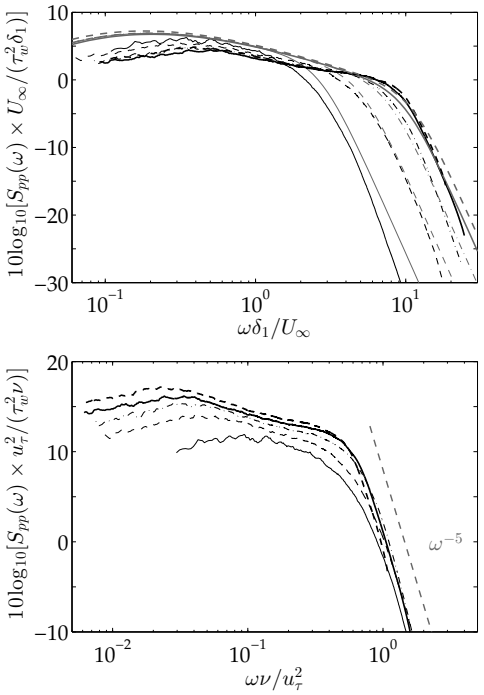

Figure 2. Measured wall pressure spectra for a zero-pressure-gradient boundary layer. —— zpg11 case, – – – zpg25 case, –·–·– zpg36 case, —— zpg45 case, **– – –** zpg59 case, refer to Table 1 for boundary layer parameters. On the top, spectra normalized by mixed variables and comparison with Goody's model (Goody, 2004) in grey. On the bottom, spectra normalized by inner variables and comparison with the ω^{-5} power law.

Casarella (1991) using the following empirical law

$$p_w^{+2} = \begin{cases} 6.5 & (\mathrm{Re}^+ \le 333) \\ 6.5 + 1.86\log(\mathrm{Re}^+/333) & (\mathrm{Re}^+ > 333) \end{cases}$$

In the present experiment, increasing the mean pressure gradient leads to an increase in p_w^+. For the apg configuration, p_w^+ is of the order of 5, whereas it is of the order of 3 for the zpg configuration, and of 2 for the fpg configuration.

WAVENUMBER-FREQUENCY SPECTRA

Signal Processing

The linear antenna consists of $n_p = 63$ identical remote microphones, in order to reach a spacing of 1 mm between probes near the antenna center. These probes are non-uniformly distributed along the disk diameter, to enhance the spectral resolution. For each angular position of the rotating array, pressure signals are recorded for the n_p microphones, at a sampling frequency of 51.2 kHz during a time length $T_0 = 90$ s. The two-sided cross-spectrum R_{ij} between two probes located at $\boldsymbol{x}$ and $\boldsymbol{x} = \boldsymbol{x} + \boldsymbol{r}$ is defined as

$$R(\boldsymbol{r},\omega) = \lim_{T\to\infty} \frac{2\pi}{T} E\left[\hat{p}(\boldsymbol{x},\omega)\hat{p}^\star(\boldsymbol{x}+\boldsymbol{r},\omega)\right]$$

for homogeneous turbulence, where $\hat{p}(\boldsymbol{x},\omega)$ is the Fourier transform of $p(\boldsymbol{x},t)$, $\hat{p}^\star$ is the conjugate of $\hat{p}$, and E is the

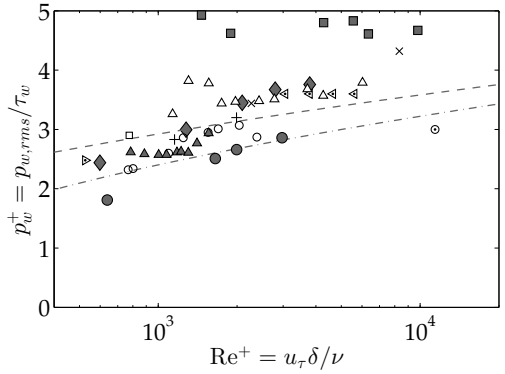

Figure 3. Normalized root mean square wall pressure fluctuations p_w^+ as a function of the Reynolds number Re^+. ZPG-BL: ♦ present data, ∘ Corcos (1964), □ Emmerling *et al.* (1973), ◁ Blake (1970), ▷ Schewe (1983), △ McGrath & Simpson (1987), ○ Gravante *et al.* (1998), + and – – – from Farabee & Casarella (1991), × Goody & Simpson (2000), –·–·– Viazzo *et al.* (2001). APG-BL: ■ present data. FPG-BL: ● present data, ▲ McGrath & Simpson (1987) for $-0.48 \le \beta \le -0.16$.

mathematical expectation (Bendat & Piersol, 2010). All these cross-spectra are calculated by splitting the time signal into $m_t = 360$ blocks of time length $T = 250$ ms, without any overlap between the blocks. No windowing function has been applied to the data blocks. It has been found more efficient to apply a moving average to cross-spectra with a filter width Δf proportional to the frequency, namely $\Delta f = f/10$.

The wavenumber-frequency spectrum is then obtained by taking the 2-D Fourier transform of the cross-spectra

$$\Phi_{pp}(\boldsymbol{k},\omega) = \frac{1}{(2\pi)^2}\iint R(\boldsymbol{r},\omega)e^{-i\boldsymbol{k}\cdot\boldsymbol{r}}d\boldsymbol{r}$$

over the antenna disk. The reconstruction of $\Phi_{pp}(\boldsymbol{k},\omega)$ is undertaken in polar coordinates. The transducer locations are denoted by $\boldsymbol{r}_{nm} = (d_n,\theta_m)$, where $0 \le n \le n_r$ with $d_n > 0$, and the angular antenna position is given by $\theta_m = m\Delta\theta$, with $\Delta\theta = \pi/m_\theta$ and $m_\theta = 63$. The wavevector-frequency spectrum is then calculated by considering half a turn of the antenna, and both directions of the linear array, that is θ_m and $\theta_m + \pi$. It yields

$$\begin{aligned}\Phi_{pp}(\boldsymbol{k},\omega) \;=\; & \frac{1}{(2\pi)^2}\sum_{m=0}^{m_\theta-1}\sum_{n=0}^{n_r}\left[R(\boldsymbol{r}_{nm},\omega)e^{-i\boldsymbol{k}\cdot\boldsymbol{r}_{nm}}\right. \\ & \left. +\; R(-\boldsymbol{r}_{nm},\omega)e^{+i\boldsymbol{k}\cdot\boldsymbol{r}_{nm}}\right]ds_n \qquad (1)\end{aligned}$$

By noting that $R(-\boldsymbol{r}_{nm},\omega) = R^\star(\boldsymbol{r}_{nm},\omega)$, the previous expression can be simplified to $2\Re\left[R(\boldsymbol{r}_{nm},\omega)e^{-i\boldsymbol{k}\cdot\boldsymbol{r}_{nm}}\right]$ for the integrand. In a previous study (Arguillat *et al.*, 2010), the central microphone was taken as the reference, and each half of the linear antenna is associated with θ_m and $\theta_m + \pi$ respectively. The cross-spectrum $R(\boldsymbol{r},\omega)$ is then discretized by $n_r = (n_p - 1)/2 = 31$ points in the radial direction.

In the present work, the wavenumber-frequency spectrum is reconstructed by making use of all the possible distances between two probes in one direction, under the assumption of homogeneous turbulence. There are potentially

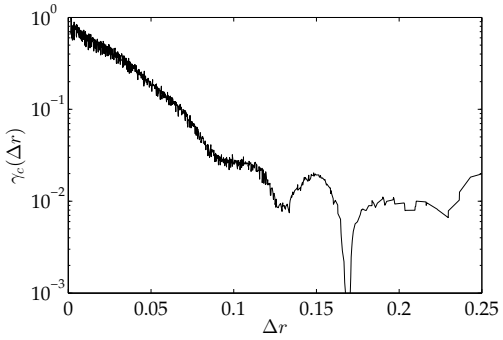

Figure 4. Amplitude of the coherence function $\gamma_c(\Delta r) = |R(\boldsymbol{r},\omega)|/\sqrt{S_{pp}(0,\omega)S_{pp}(\boldsymbol{r},\omega)}$ reconstructed in the radial direction along the mean flow ($\theta = 0$) at $f = 10^3$ Hz, for the case zpg45.

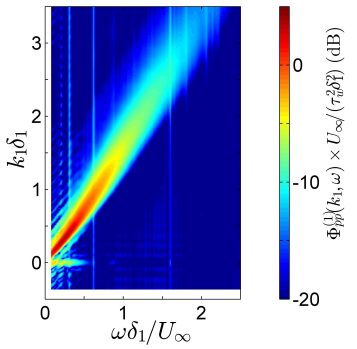

Figure 5. Normalized streamwise one-dimensional spectrum $\Phi_{pp}^{(1)}(k_1,\omega)\times U_\infty/(\tau_w{}^2\delta_1{}^2)$ in dB, as a function of the reduced frequency $\omega\delta_1/U_\infty$ and of streamwise wavenumber $k_1\delta_1$ for the case zpg45.

$n_p(n_p-1)/2$ couples, and by removing redundancies, the cross-spectrum $R(\boldsymbol{r},\omega)$ in the radial direction along the linear antenna is estimated from $n_r = 855$ pairs. As an illustration, the coherence function $\gamma_c(\Delta r)$ reconstructed in the radial direction along the mean flow, and at a given frequency, is shown in Fig. 4.

The elementary area ds_n is calculated as $ds_n = \pi(l_{n+1}^2 - l_n^2)\times\Delta\theta/2\pi$ with $l_n = d_n + d_{n+1}/2$, and a Hann windowing is applied in the radial direction for the space integration. The spectral resolution $2\pi/d_a$ is imposed by the antenna diameter d_a, and a spectral grid with a regular step of $\Delta k = 5$ m^{-1} has been chosen. Finally, note that $\Phi_{pp}(\boldsymbol{k},\omega)$ is a real quantity, that is $\Phi_{pp}(\boldsymbol{k},\omega) = \Phi_{pp}^{\star}(\boldsymbol{k},\omega)$.

1-D Spectra

Streamwise one-dimensional wavenumber-frequency spectra $\Phi_{pp}^{(1)}(k_1,\omega)$ are defined by integrating the 2-D spectra over the transverse wavenumbers,

$$\Phi_{pp}^{(1)}(k_1,\omega) = \int_{-\infty}^{+\infty}\Phi_{pp}(k_1,k_2,\omega)dk_2$$

This spectrum is shown for the zpg45 case in Fig. 5, by noting that $\Phi_{pp}^{(1)}(k_1,\omega) = 2\pi\Phi_{pp}^{(1)}(k_1,f)$. The convective ridge located around the convective wavenumber $k_1 = k_c = \omega/U_c$, follows a slightly concave curve for the higher values of the frequency. This indicates that the convection velocity U_c is progressively reduced when the frequency increases, which is consistent with other experimental data and also with the predictions of a modified Smolyakov model (Salze *et al.*, 2014). A second contribution is also visible, less energetic and following a line very slightly inclined relative to the frequency axis. This a trace of the acoustic contribution to the wall pressure field (Abraham & Keith, 1998).

2-D Spectra

The normalized wavenumber-frequency pressure spectrum is plotted in Fig. 6 for the case zpg45, and for 6 dimensionless frequencies from $\omega\delta_1/U_\infty = 0.26$ to 1.55, corresponding to $500 \le f \le 3000$ Hz. The turbulent or aerodynamic part, centered around the convective wavenumber $k_1 = k_c$ is clearly seen with its characteristic elongated shape in the k_2 direction. The dissymmetry in the k_1 direction is also apparent. The spoke pattern is generated by the polar Fourier transform, and can be explained theoretically (Coggins & Zhou, 2006). The acoustic component is seen as a circle centered around the origin and of radius $k_0 = \omega/c_\infty$. More precisely, from the geometrical acoustic dispersion relation $c_\infty^2k^2 - (k_1U_\infty - \omega)^2 = 0$, it can been shown that the acoustic domain lies inside the ellipse given by

$$\frac{(k_1 + (M/\beta^2)k_0)^2}{(k_0/\beta^2)^2} + \frac{k_2^2}{(k_0/\beta)^2} = 1$$

where $M = U_\infty/c_\infty$ is the free stream Mach number and $\beta = \sqrt{1-M^2}$ is the Prandtl-Glauert parameter. However, the velocity is quite moderate in the present case, and $\beta \simeq 1$.

The energy ratio between the convective and the acoustic parts is now examined. The acoustic contribution, identified from the dispersion relation of acoustic waves, is integrated in wavenumber space over the acoustic disk. The ratio η of the acoustic part relative to the total pressure field is shown in Fig. 7, as a function of the frequency. With respect to the discretization in wavenumber space, η can be correctly estimated only for frequencies $\omega\delta_1/U_\infty \ge 0.28$. One has $\eta \simeq 0.01 - 0.02$ for the zpg45 configuration. The difference between the total pressure field and the acoustic contribution is about 20 dB.

CONCLUDING REMARKS

Wall pressure fluctuations beneath a turbulent boundary layer submitted to an external pressure gradient have been investigated. Wall pressure fluctuations have been measured using a pinhole microphone. They are in good agreement with previous experimental data, and also with the semi-empirical model of Goody for the zpg configuration. An effort is under way to develop a less empirical model, with the aim to introduce the influence of a pressure gradient.

Wavevector-frequency spectra have also been performed from the use of a rotating linear array of remote microphones, for which the distribution is optimized to enhance the spectral resolution. They are estimated by taking the 2-D Fourier transform of the measured cross-spectra, and by using all the possible pairs associated with the irregular distribution of the probes along the linear antenna. The

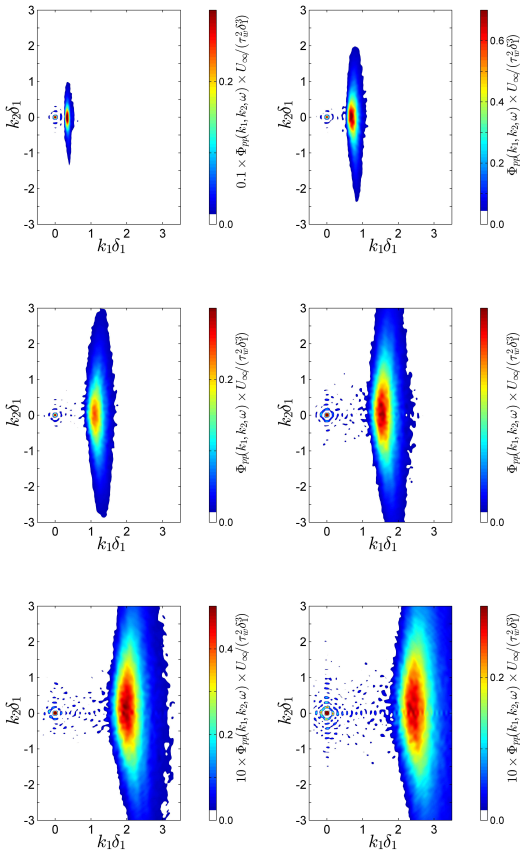

Figure 6. Wavenumber-frequency spectra for the zpg45 case at $\omega = 0.26$ (500 Hz), 0.52, 0.77, 1.03, 1.29 and 1.55 (3000 Hz), using a linear scale for amplitude.

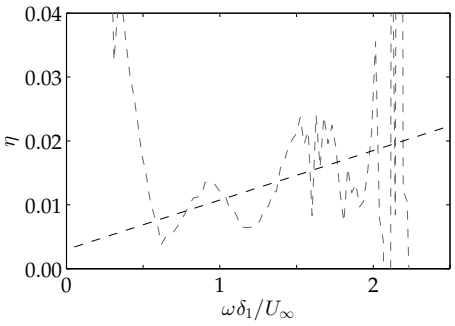

Figure 7. Contribution of the acoustic part relative to the total field $\Phi_{pp}(\boldsymbol{k},\omega)$, as a function of the normalized frequency $\omega\delta_1/U_\infty$.

acoustic part can be separated from the convective one in a reasonable range of frequencies. Despite the limited spectral resolution, the acoustic contribution can be integrated in wavenumber space to estimate its relative contribution to the total pressure field.

Work is in progress to determine the influence of adverse and of favorable external pressure gradients, and the relative contribution of the acoustic component to the wall pressure field.

Acknowledgments

This research has been funded by the Agence Nationale de la Recherche through the ANR-2011- BS09-035-02 project SONOBL, and by the Labex CeLyA of Université de Lyon, operated by the French National Research Agency (ANR-10-LABX-0060/ ANR-11-IDEX-0007).

REFERENCES

Abraham, B. M. & Keith W. L., 1998, Direct measurements of turbulent boundary layer wall pressure wavenumber-frequency spectra, *J. Fluid Eng.*, **120**, 29-39.

Arguillat, B., Ricot, D., Bailly, C. & Robert, G., 2010, Measured wavenumber - frequency spectrum associated with acoustic and aerodynamic wall pressure fluctuations, *J. Acoust. Soc. Am.*, **128**(4), 1647-1655.

Blake, W. K., 1970, Turbulent boundary-layer wall-pressure fluctuations on smooth and rough walls, *J. Fluid Mech.*, **44**(4), 637-660.

Blake, W. K., 1986, Essentials of turbulent wall-pressure fluctuations, in Mechanics of flow-induced sound and vibration, Vol. II Complex flow-structure interactions, *Academic Press Inc.*, Orlando, Florida.

Bremner, P., 2014, Developing aerodynamic design diagnostics for control of interior wind noise, Proceedings of the 14ème Congrès Français d'Acoustique, Poitiers, France, 2139-2146.

Bendat, J.S. & Piersol, A.G., 2010, *Random Data*, Fourth Edition, Wiley. Refer to Chapter 5.

Bull, M. K., 1996, Wall-pressure fluctuations beneath turbulent boundary layers: some reflections on forty years of research, *J. Sound Vib.*, **190**(3), 299-315.

Cipolla, K. & Keith, W., 2000, Effects of pressure gradients on turbulent boundary layer wave number frequency spectra, *AIAA Journal*, **38**(10), 1832-1836.

Coggins, B. E. & Zhou, P., 2006, Polar Fourier transforms of radially sampled NMR data, *Journal of Magnetic Resonance*, **182**, 84-95.

Corcos, G. M., 1963, Resolution of pressure in turbulence, *J. Acous. Soc. Am.*, **35**(2), 192-199.

Corcos, G. M., 1964, The structure of the turbulent pressure field in boundary-layer flows, *J. Fluid Mech.*, **18**(3), 353-378.

Ehrenfried, K. & Koop, L., 2008, Experimental study of pressure fluctuations beneath a compressible turbulent boundary layer, 14th AIAA/CEAS Aeroacoustics Conference, AIAA Paper 2008-2800.

Emmerling, R., Meier, G. E. A. & Dinkelacker, A., 1973, Investigation of the instantaneous structure of the wall pressure under a trubulent boundary layer flow, *Agard*, Conference Proceedings No. 131, on Noise Mechanisms, 21-1 - 24-12.

Farabee, T. M. & Casarella, M. J., 1991, Spectral features of wall pressure fluctuations beneath turbulent boundary layer, *Phys. Fluids A*, **3**(10), 2410-2420.

Gabriel, C., Müller, S., Ullrich, F. & Lerch, R., 2014, A new kind of sensor arry for measuring spatial coherence of surface pressure on a car's side window, *J. Sound Vib.*, **333**, 901-915.

Gloerfelt, X. & Berland, J., 2013, Turbulent boundary-layer noise: direct radiation at Mach number 0.5, *J. Fluid Mech.*, **723**, 318-351.

Goody, M. C. & Simpson, R. L., 2000, Surface pressure fluctuations beneath two- and three-dimensional turbulent boundary layers, *AIAA Journal*, **38**(10), 1822-1831.

Goody, M., 2004, Empirical spectral model of surface pressure fluctuations, *AIAA Journal*, **42**(9), 1788-1794.

Graham, W. R., 1997, A comparison of models for the wavenumber-frequency spectrum of turbulent boundary layer pressures, *J. Sound Vib.*, **206**(4), 430-454.

Gravante, S. P., Naguib, A. M., Wark, C. E. & Nagib, H. M., 1998, Characterization of the pressure fluctuations under a fully developed turbulent boundary layer, *AIAA Journal*, **36**(10), 1808-1816.

Hu, Z., Morfey, C. L. & Sandham, N. D., 2006, Sound radiation from a turbulent boundary layer, *Phys. Fluids*, **18**, 098101, 1-4.

Keith, W. L., Hurdis, D. A. & Abraham, B. M., 1992, A comparison of turbulent boundary layer wall-pressure spectra, *Journal of Fluids Engineering*, **114**, 338-347.

Kremer, F., Bogey, C. & Bailly, C., 2014, Semi-implicit Runge-Kutta schemes: development and application to compressible channel flow, *AIAA Journal*, **52**(3), 516-527.

Leclercq, D. J. J. & Bohineust, X., 2002, Investigation and modelling of the wall pressure field beneath a turbulent boundary layer at low and medium frequencies, *J. Sound Vib.*, **257**(3), 477-501.

McGrath, B. E. & Simpson, R. L., 1987, Some features of surface pressure fluctuations in turbulent boundary layers with zero and favorable pressure gradients, NASA-CR-4051.

Panton, R. L. & Robert, G., 1994, The wavenumber-phase velocity representation for the turbulent wall-pressure spectrum, *Journal of Fluid Engineering*, **480**(116), 477-483.

Salze, E., Bailly, C., Marsden, O., Jondeau, E. & Juvé, D., 2014, An experimental characterization of wall pressure wavenumber-frequency spectra in the presence of pressure gradients, 20th AIAA/CEAS Aeroacoustics Conference, AIAA Paper 2014-2909.

Schewe, G., 1983, On the structure and resolution of wall-pressure fluctuations associated with turbulent boundary-layer flow, *J. Fluid Mech.*, **134**, 311-328.

Schloemer, H. H., 1967, Effects of pressure gradient on turbulent-boundary-layer wall-pressure fluctuations, *J. Acoust. Soc. Am.*, **42**(1), 93-113.

Sevik, M. M., 1986, Topics in hydro-acoustics, in *Aero- and Hydro-Acoustics*, Springer-Verlag Berlin, 285-308.

Viazzo, S., Dejoan, A. & Schiestel, R., 2001, Spectral features of the wall-pressure fluctuations in turbulent wall flows with and without perturbations using LES, *Int. J. Heat Fluid Flow*, **22**, 39-52.

Wilby, J. F., 1996, Aircraft interior noise, *J. Sound Vib.*, **190**(3), 545-564.